Different origins of seafloor undulations in a submarine canyon system, northern South China Sea, based on their seismic character and relative location

Jian Li[a, b], Wei Li[a, b]*, Tiago M. Alves[c], Michele Rebesco[d], Wenhuan Zhan[a, b], Jie Sun[a], Neil C. Mitchell[e], Shiguo Wu[f]

[a] CAS Key Laboratory of Ocean and Marginal Sea Geology, South China Sea Institute of Oceanology, Chinese Academy of Sciences, Guangzhou 510301, P.R. China

[b] University of Chinese Academy of Sciences, Beijing 100049, P.R. China

[c] 3D Seismic Lab, School of Earth and Ocean Sciences, Cardiff University, Main Building, Park Place, Cardiff, CF10 3AT, United Kingdom

[d] Instituto Nazionale di Oceanografia e di Geofisica Sperimentale (OGS), Borgo Grotta Gigante 42/C, Sgonico, 34010 Trieste, Italy

[e] School of Earth and Environmental Sciences, The University of Manchester, Manchester M13 9PL, UK

[f] Institute of Deep-sea Science and Engineering, Chinese Academy of Sciences, Sanya 572000, P.R. China

*Correspondence to: Dr. Wei Li (wli@scsio.ac.cn)

Abstract

High-resolution 2D and 3D seismic data are used to investigate the morphology, internal architecture and origin of widespread seafloor undulations in the eastern area of a submarine canyon system, northern South China Sea. The seafloor undulations reveal similar seafloor morphologies, and three different types (Types A, B and C) can be classified based on their relative locations and internal seismic characters. Types A

and B are observed in the canyon areas, whereas Type C occurs in the canyon heads. Seismic reflections within Types A and C are continuous and have an upslope migrating trend, while Type B seafloor undulations are separated by listric faults. Our analysis reveals the origins of these three different types of seafloor undulations. Type A seafloor undulations are sediment waves formed by turbidity currents flowing through the submarine canyons. Gravity-driven submarine creep resulted in the formation of Type B seafloor undulations. Type C undulations are sediment waves generated by internal waves interacting with the continental slope. Our results provide information about the origin of widespread seafloor undulations in other submarine canyon systems. It is also of great significance to future risk assessments, as the study area now is one of the most active regions for hydrocarbon exploration in SE Asia.

Keywords: South China Sea; Submarine canyons; Seafloor undulations; Bathymetry; Internal seismic character.

1 Introduction

Seafloor undulations are one of the most widespread bedforms on both passive and active continental margins (Symons et al., 2016), revealing a wide range of morphologies, dimensions and sediment types (Ribó et al., 2018). Seafloor undulations are generated by a combination of depositional and erosional processes, and their crests comprise positive features relative to the surrounding seafloor (Symons et al., 2016). Seafloor undulations have been documented in a wide range of

47 submarine settings, including on continental shelves (Belde et al., 2017), continental
48 slopes (Ribó et al., 2018), continental rises (Gonthier et al., 2002), abyssal plains
49 (Baldwin et al., 2017), the slopes of volcanic islands (Pope et al., 2018), and
50 submarine canyons and channels (Gong et al., 2012). Seafloor undulations are
51 commonly associated with sediment waves and sediment deformation under
52 gravity-driven submarine creep (Wynn and Stow, 2002).

53 Sediment waves can be created by along-slope bottom currents, downslope
54 turbidity currents or by a combination of both their processes (Wynn and Stow, 2002;
55 Symons et al., 2016). Sediment waves formed by bottom currents are chiefly related
56 to sediment drifts, with their wavelength and height reaching up to 10 km and 150 m,
57 respectively (Flood et al., 1993; Wynn and Stow, 2002; Rebesco et al., 2007).
58 Sediment waves formed by turbidity currents are common in channel levees, canyon
59 and channel mouths, and typically reveal wavelengths and heights of up to 7 km and
60 80 m, respectively (Wynn and Stow, 2002). Sediment waves can also be generated by
61 internal waves (Karl et al., 1986; Reeder et al., 2011; Ribó et al., 2016), and have been
62 found in the heads of submarine canyons. Here, they show average wave heights of 5
63 m and wavelengths of up to 650 m (Karl et al., 1986). Sediment waves have been
64 widely documented on the northern South China Sea margin, especially in the
65 Qiongdongnan (Jiang et al., 2013; Chen et al., 2017) and Taixinan Basin (Damuth,
66 1979; Gong et al., 2012; Kuang et al., 2014).

67 Apart from sediment waves formed by depositional and oceanographic processes,
68 seafloor creep can also generate vast fields of undulations where slope gradients and

sedimentation rates are relatively high (Lee and Chough, 2001; Faugeres et al., 2002; Rebesco et al., 2009; Shillington et al., 2012; Li et al., 2016a). They can generate waves up to 10 km in length and 100 m in height (Wynn and Stow, 2002). Seafloor creeping can involve into large-scale submarine landslides, posing major geohazards to infrastructure such as telecommunication cables and pipelines (Lee and Chough, 2001; Shillington et al., 2012). Therefore, it is of great importance to correctly identify the origin of seafloor undulations, and to understand the tectonic, sedimentary and oceanographic setting in which they occur (Shillington et al., 2012; Belde et al., 2017).

A large-scale submarine canyon system, consisting of eighteen regular spaced, linear, sub-parallel submarine canyons, has been previously documented on the continental slope of the Pearl River Mouth Basin (He et al., 2014; Ma et al., 2015; Li et al., 2016b) (Figs. 1 and 2). The study area in this work is situated in the eastern part of this submarine canyon system at water depths between 600 and 1600 m (Fig. 2). Here, seafloor undulations are broadly distributed in the thalwegs, flanks and heads of the studied submarine canyons, and doubts still exist on their origin and formation processes. The seafloor undulations in the heads and flanks of the canyons have been proposed to reflect seafloor creep and landslides (He et al., 2014). However, Qiao et al. (2015) considered that seafloor undulations in the heads of the canyons relate to creep folds induced by soft sediment deformation, while waves in the lower segment of canyons are associated to turbidity currents overflowing their thalwegs. Additionally, seafloor undulations in the heads and on the flanks of canyons are

caused by sediment deformation (Li et al., 2016b). Ma et al. (2015) also interpreted seafloor undulations in the heads and flanks of submarine canyons as failure scars. Notwithstanding these differing interpretations, it is of great importance to determine the exact origin and formation processes of these seafloor undulations, and their implications for future geohazard assessments. The study area is now one of the most active deep-water regions for hydrocarbon exploration on the northern South China Sea margin. In this study, a combination of 2D and 3D seismic data, and high-resolution bathymetry derived from 3D seismic data, are used to:

(a) investigate the morphology of the seafloor undulations;

(b) describe their detailed internal architectures on high-resolution seismic profiles;

(c) determine the origin of seafloor undulations in different segments of submarine canyons;

(d) discuss the implications of identifying seafloor undulations on continental margins.

2 Geological setting

The South China Sea (SCS) is located at the junction between the Pacific, the Indian-Australian, and the Eurasian tectonic plates, being the largest and deepest marginal sea in the western Pacific Ocean (Taylor and Hayes, 1980). Several major sedimentary basins occur along its northern margin, such as the Yinggehai, Qiongdongnan, Pearl River Mouth, and Taixinan Basins (Xie et al., 2006) (Fig.1). As

113 the largest deep-water basin in the northern South China Sea, the Pearl River Mouth
114 Basin is also one of the most important petroliferous regions of China (Dong et al.,
115 2009; Zhu et al., 2009).

116 The Baiyun Sag is an intraslope basin, with a water depth ranging from 200 to
117 2000 m, part of the larger Pearl River Mouth Basin (Zhu et al., 2010). A submarine
118 canyon system consisting of eighteen submarine canyons is the most prominent
119 geomorphologic feature of the Pearl River Mouth Basin (Figs. 1 and 2). This
120 submarine canyon system records four evolutionary phases based on its internal
121 seismic facies and spatial distribution (Ma et al., 2015): (1) small individual channels
122 were initially formed in the middle of the Baiyun Sag (13.8-12.5 Ma); (2) channels
123 were enlarged in a second stage because decreasing sediment input and stable tectonic
124 subsidence in the Baiyun Sag increased the slope angle(12.5-10.5 Ma); (3) channels
125 were broadly distributed and covered the entire Baiyun Sag due to a further decrease
126 in sediment input, with the Dongsha Event later enhancing the flow of gravity
127 currents (10.5-5.5 Ma); (4) channel incision ceased in the northeastern Baiyun Sag,
128 while channels continued to develop in the study area to form modern features (5.5-0
129 Ma). In the study area, submarine canyons migrated unidirectionally to the NE from
130 the middle Miocene to the present day due to the continued action of gravity and
131 bottom currents (Zhu et al., 2010; Gong et al., 2013; Jiang et al., 2017; Gong et al.,
132 2018).

133 Three major water masses exist at different depths on the northern South China
134 Sea (Fig. 1).They comprise seasonal surface water masses (at < 350 m water depth),

intermediate water masses (between 350 m and 1350 m water depth), and deep-water masses (at > 1350 m water depth) (Chen and Wang, 1998; Chen, 2005; Zhu et al., 2010; Gong et al., 2013). The study area is mainly affected by intermediate water and deep-water masses. Intermediate water, itself sourced from the North Pacific intermediate water, is considered to have an anti-cyclonic flow that was established in the late Miocene. It is characterised by salinity values between 34.35 and 34.43, with temperature ranging from 7 to 10°C (Chen and Wang, 1998; Chen, 2005; Yang et al., 2010; Chen et al., 2014). Deep-water masses associated with the southwestward flow of the Northern Pacific Deep Water through the Luzon Strait, have a cyclonic circulation. Deep-water circulation was established in the late Miocene and gradually evolved into the modern pattern at ~1.0 Ma (Ludmann et al., 2005; Chen et al., 2014). At present, the velocity of deep-water masses generally varies between 0-2cm/s based on *in situ* observations (Zhao et al., 2015).

Internal waves in the northern South China Sea are the largest waves documented in the world's oceans (Zhao et al., 2004; Li et al., 2011; Alford et al., 2015). Active internal wave fields in the northern South China Sea occur in the vicinity of the Dongsha Island and Shenhu Ansha shoal (Fig. 1). Remote sensing studies suggest that internal waves originate either from the local continental shelf break, or from the Luzon Strait on the eastern margin of the South China Sea, as a result of interactions between strong tides and local bathymetric features (Zhao et al., 2004; Li et al., 2008). These internal waves propagate into shallow waters and ultimately dissipate on the continental shelf (Li et al., 2011; Reeder et al., 2011; Ma et

157 al., 2016).

158

159 **3 Data and methods**

160 The dataset used in this study consist of high-resolution bathymetric data derived
161 from 3D seismic and 2D/3D seismic profiles (Figs. 2 and 3). The seismic data were
162 acquired by China National Offshore Oil Corporation using a 3000-m long streamer
163 with 240 channels. The 3D seismic volumes were collected with a sampling interval
164 of 4 ms and processed with a bin spacing of 12.5 m × 25 m in their cross-line and
165 inline directions, respectively. The frequency bandwidth of the seismic data is 30–45
166 Hz, providing an average vertical resolution of 8–10 m for the depth of occurrence of
167 seafloor undulations. The vertical scale for all the seismic profiles used in this study is
168 two-way travel time (TWT). Schlumberger's Geoframe® 4.5 software was used to
169 visualise and interpret the seismic data.

170 The interpreted high-resolution bathymetric data covers the submarine canyon
171 system of the Pearl River Mouth Basin in almost its entirety. Horizontal and vertical
172 resolutions for the bathymetric data are ~100 m and 3–6 m, respectively. This
173 resolution is sufficient to gather information on the dimensions, water depths and
174 orientations of large-scale bedforms on the continental slope (Figs. 2 and 3).

175

176 **4 Results**

177 **4.1 Seafloor morphology**

178 **4.1.1 General geomorphology**

High-resolution bathymetric data shows that the continental slope has an inclination of ~2° between 300 m and 1600 m water depth (Figs. 2 and 3). The submarine canyons on the continental slope are connected to the wide continental shelf and deep-water basin, and are named in this work, from southwest to northeast, as C1 to C18 (Fig.2). All submarine canyons are roughly perpendicular to the continental slope, and show a NW-SE orientation. Submarine canyons have lengths of 15-40 km, widths ranging from 2 to 5 km, and incision depths of 100-350 m (Fig.2). Flanking strata between the submarine canyons become gradually narrower in the downslope direction(Fig.2).

The high-resolution bathymetric map shows that the seafloor in the heads and flanks of the westernmost submarine canyons C1 to C8 is relatively smooth compared to the easternmost submarine canyons (C9-C18). The heads of canyons C9 to C18 are rough and characterised by widespread seafloor undulations. In addition, multiple slide scarps are observed in the downslope region of the submarine canyons (Fig. 2). The dimensions of these slide scarps range from hundreds of meters to several kilometres in length, and can be dozens of meters in height (Fig. 2).

4.1.2 Morphological description of the seafloor undulations

Seafloor undulations are chiefly located in the canyon thalwegs, flanks and heads of Canyons C9 to C18 (Figs. 2 and 3).

(a) Seafloor undulations on the canyon flanks and lower slope

Compared to seafloor undulations at the canyon heads, undulations on the flanks and lower slope are smaller and more complex in plan view (Figs. 2 and 3). It is difficult to trace the crests of the seafloor undulations on the bathymetric map. However, the bathymetric profiles reveal that the wavelength (measured from trough to trough) of seafloor undulations varies from 1 km to 2 km on the canyon flanks and lower slope (Fig. 4). Wave height ranges from 50 m to 100 m. In addition, a series of slide scars are observed on the canyon flanks (Fig. 2).

(b) Seafloor undulations in the canyon heads

Multiple seafloor undulations were identified in the heads of the canyons at a water depth between 600 m and 900 m. Their strikes are roughly perpendicular to the canyon axis (Figs. 3 and 5a). The crests of the seafloor undulations (see red lines in Fig 3b), are generally parallel or sub-parallel to the bathymetric contours. In addition, the crests of the seafloor undulations show no clear bifurcation in plan view. Topographic profiles crossing the head of the canyons reveal a variety of dimensions with wavelength ranging from 0.8 km to 1.5 km (Fig. 5). Wave height ranges from 20 m to50 m.

4.2 Seismic characteristics of the seafloor undulations

Several high-resolution seismic profiles crossing the thalwegs, flanks and heads of the submarine canyon system image the internal architecture of the seafloor undulations (Fig. 2). The seafloor undulations can therefore be divided into three main

types, A, B and C, based on their internal architecture and relative locations in the submarine canyon system.

4.2.1 Type A seafloor undulations

Type A undulations are observed in the lower segments of the canyon thalwegs (Figs. 3, 6 and 7). The sedimentary succession affected by the undulations has a thickness of ~200 ms TWT (Fig.7). Seismic profiles show that most seismic reflections are continuous, and can be traced from one wave to the next (Figs. 6 and 7). However, multiple mass-transport deposits (MTDs), characterised by discontinuous and chaotic internal seismic reflections, are also observed, proving that important sediment instability has occurred in the lower segment of the canyon thalwegs (Fig.7).

Discrete undulations reveal an asymmetric morphology with gentle upslope flanks and steep downslope flanks (Fig. 7). They are commonly thicker on their upslope flanks. Undulations show a marked trend for upslope migration (Fig.7b). Deeply buried undulations show relatively shorter upslope flanks and longer downslope flanks (Fig. 7). In contrast, the upslope flanks of shallow-buried undulations are longer than their downslope counterparts (Fig. 7). Downslope flanks also reveal erosional truncations in shallow-buried undulations (Fig. 7).

4.2.2 Type B seafloor undulations

Type B undulations occur on the canyon flanks, further upslope when compared to Type A. High-resolution seismic lines crossing the canyon flank between C11 and

C12 reveal the internal architecture of Type B undulations (Figs. 2, 6, 8 and 9). The sedimentary succession affected by these undulations has a thickness of ~200 ms TWT. A series of high-amplitude (enhanced) seismic reflections can be identified along the base of the undulations (Figs. 6, 8 and 9a). They are usually distributed around, or above, focused fluid-flow structures such as gas chimneys (Figs. 8 and 9a).

Seismic reflections in Type B undulations are not continuous and cannot be traced across the troughs separating distinct sediment waves. Most of these undulations are separated by listric faults (Figs. 6, 8 and 9). The troughs of the undulations are related to displacements of ~100ms TWT along the fault planes (Fig. 9).

Type B undulations are characterised by their asymmetric morphology (Fig. 9). Upslope flanks reveal sub-parallel seismic reflections, whereas their downslope flanks are thin and show erosional truncation within shallow undulations (Fig. 9). The crests of Type B undulations also show an apparent upslope migration trend.

4.2.3 Type C seafloor undulations

Type C undulations are observed close to the heads of the canyons. The thickness of the strata affected by Type C undulations decreases from ~200 ms TWT to ~100 ms TWT in a downslope direction (Figs. 6, 10 and 11). Type C undulations are characterised by their wavy, asymmetric morphology and laterally continuous seismic reflections, although chaotic seismic reflections can also be identified due to the presence of MTDs (Fig. 11b). The upslope flanks of the undulations are characterised

by aggradation, whereas their downslope flanks are dominated by erosion and non-deposition. Thus, the crests of Type C undulations reveal an upslope migration trend with time. Note that some of shallow buried undulations reveal erosional truncation on their downslope flanks (Fig. 10a).

5 Discussion

5.1 Genesis of widespread seafloor undulations in a submarine canyon system

Seafloor undulations have been observed in submarine canyon systems all around the world (Gonthier et al., 2002; Gong et al., 2012; Ribó et al., 2018). Four main hypotheses have been proposed for their genesis based on the environment settings in which seafloor undulations occur, their morphological characteristics, and internal architectures. These four hypotheses include: (1) bottom currents (Masson et al., 2002; Baldwin et al., 2017; Belde et al., 2017); (2) turbidity currents (Lewis and Pantin, 2002; Normark et al., 2002; McCave, 2017); (3) internal waves (Karl et al., 1986; Droghei et al., 2016; Ma et al., 2016; Ribó et al., 2016); and (4) gravity-driven downslope submarine creeps (Lee and Chough, 2001; Shillington et al., 2012; Li, et al., 2016a). In the following sections, the formation mechanisms of seafloor undulations are discussed for the study area based on the criteria proposed by Wynn and Stow (2002) and Symons et al. (2016).

5.1.1 Origin and formation process of Type A seafloor undulations(canyon thalwegs)

Turbidity currents are major downslope sediment transport processes, and are commonly identified in submarine canyons, channels and gullies (Shepard, 1981; Parker, 1982; Canals et al., 2006; Talling et al., 2015; Paull et al., 2018). Sediment waves generated by turbidity currents have been documented in regions such as the Monterey Fan channel (Normark et al., 1980), on the South Iberian Margin (Alves et al., 2003; Perez-Hernandez et al., 2014) and in the northern South China Sea (Gong et al., 2012; Jiang et al., 2013).

In the study area, Type A undulations are closely linked to the lower segments of the canyon thalwegs (Figs. 26 and 7). Internal seismic reflections within the undulations are continuous and can be traced from one wave to the next (Figs. 6 and 7). Each undulation reveals an asymmetric morphology, with gentle upslope flanks and steep downslope flanks (Fig. 7). All these undulations show a significant trend of upslope migration as their upslope flanks accumulate sediment more rapidly than their downslope flanks (Fig. 7). Based on criteria proposed by Wynn and Stow (2002), Type A undulations are similar to sediment waves generated by turbidity currents, e.g. the Selvagens sediment-wave field, NE Atlantic (Wynn et al., 2000), and the Hikurangi Trough east of New Zealand (Lewis and Pantin, 2002).

Our study area is located on the continental slope of the northern South China Sea. In this region, multiple submarine instability features, i.e. creeps, slumps and

311 landslide complexes, are developed in an area incised by multiple submarine canyons
312 (He et al., 2014; Chen et al., 2016). Previous studies suggest that turbidity currents are
313 produced by the downslope transport of slumps and mass flows (Parker, 1982; Ercilla
314 et al., 2002). Li et al. (2015) also suggest that slumps and mass flows occurred
315 frequently in the past to generate turbidity currents in submarine canyon systems of
316 the northern South China Sea margin. As discussed above, we infer that Type A
317 undulations comprise sediment waves produced by turbidity currents associated with
318 frequent slumping and mass wasting in the submarine canyons.
319
320 **5.1.2 Origin and formation processes of Type B seafloor undulations (canyon**
321 **flanks)**
322
323 The internal seismic reflections within Type B undulations are not continuous,
324 and cannot be traced across successive troughs separating the observed undulations
325 (Figs. 6, 8 and 9). These troughs are commonly associated with listric faults (Figs. 6,
326 8 and 9). Undulations are generally thicker on their upslope flanks, and thinner (or
327 even eroded) in their downslope flanks (Fig. 9). Seafloor undulations associated with
328 listric faults have been documented by Faugères et al. (2002) and Gonthier et al.
329 (2002). They were interpreted as reflecting gravity-driven downslope submarine creep.
330 The basic conditions for the formation of submarine creeps have been summarised by
331 Hill et al. (1982), including the presence of faulting and glide planes. When
332 deforming the sediments, a basal décollement zone is formed at the lower boundary of

333 the strata. Listric faults act as glide planes for the displacement of the layered
334 sediment. The regional slope gradient of submarine canyon systems varies from 1.5°
335 to 2.5°, being ~1.6° on average (He et al., 2014; Li et al., 2016b).

336 In the study area, Type B undulations are mainly located on the canyon flanks,
337 where slope gradients are steep (up to 8 degrees). Sediment drilled on the flanks of the
338 submarine canyons' lower segments consists of massive silty mud and a few sandy to
339 silty intervals with weak layers (Qiao et al., 2015). Here, soft sediment deformation
340 (submarine creep) is likely controlled by the slope gradient and strength of the
341 sediment (Wynn and Stow, 2002). Due to progressing gravity-driven downslope
342 deformation, the local accumulating of strain resulted in the development of local
343 faults within sediment waves (Liet al., 2016a). Listric faults are developed within
344 troughs, leading to significant displacement of adjacent undulations (Fig 9). Thus, we
345 interpret Type B undulations as the result of soft sediment deformation produced by
346 gravity-driven downslope submarine creep.

347 Additionally, gas chimneys, pipes, large-scale normal faults and shallow gas are
348 widespread on the lower slope of the interpreted submarine canyon system (Sun et al.,
349 2012; Chen et al., 2016). Abundant acoustic anomalies, revealed as high-amplitude
350 (enhanced) seismic reflections, can be observed close to the lower boundary of Type
351 B undulations (Figs. 6, 8 and 9a). Elsewhere, similar enhanced seismic reflections
352 have been associated with free gas and fluid accumulated in shallow strata (e.g. Sun et
353 al., 2012; 2017). Gas chimneys, pipes and faults can act as pathways for the vertical
354 migration of free gas and fluids (Sun et al., 2017). The presence of free gas and fluid

355 increases overpressure in shallow strata, and reduces its shear strength until the
356 creeping movements occur (e.g. Sultan et al., 2004; Urlaub et al., 2018).
357
358 **5.1.3 Origin and formation process of the Type C seafloor undulations (canyon**
359 **heads)**
360 Type C undulations are identified in the canyon head areas (Figs. 3, 6, 10 and 11).
361 The origin of these undulations has been interpreted in He et al. (2014), Qiao et al.
362 (2015), Ma et al. (2015), and Li et al. (2016b). Some of these authors have suggested
363 that seafloor undulations were generated by submarine soft-sediment deformation due
364 to slow gravity-driven downslope creeping (He et al., 2014; Qiao et al., 2015). Others
365 have stressed their association with failure scars and fissures (Ma et al., 2015; Li et al.,
366 2016b). Obviously, debate still exists about the origin and formation processes of
367 Type C undulations.
368 The internal seismic reflections of Type C undulations can be traced across the
369 crests and troughs of each wave in the canyon heads (Figs. 6, 10 and 11). Such an
370 internal seismic architecture suggests a depositional origin for Type C undulations,
371 rather than creeping and faulting. These undulations are similar to sediment waves
372 formed by turbidity currents on continental margins (Wynn and Stow, 2002). However,
373 the study area is located on the upper continental slope and is connected to a wide
374 continental shelf (Fig. 1). Type C undulations are widespread in the canyon heads, but
375 there is no major sediment source nearby, capable of producing unconfined turbidity
376 flows. For this reason, we consider unlikely Type C seafloor undulations to be

generated by turbidity currents.

Previous studies have considered bottom currents as an important process forming sediment waves, such as in parts of the northeast Rockall Trough (Masson et al., 2002), the Caroline Basin in the West Pacific Ocean (Baldwin et al., 2017), and even in lakes (Ceramicola et al., 2001). Bottom currents, which are associated with the North Pacific intermediate water, affect the northern South China Sea at a water depth of 350-1350 m (Chen and Wang, 1998; Chen, 2005; Zhu et al., 2010; Chen et al., 2014). Bottom currents flow to the northeast along the continental slope and affect sedimentation in the studied submarine canyon system (Zhu et al., 2010; Gong et al., 2013; Jiang et al., 2017). Sediment waves formed by bottom currents are normally oblique to the continental slope, and their crests are aligned perpendicularly or obliquely to bottom current flows (Wynn and Stow, 2002). The crests of these sediment waves are also straight or slightly sinuous, such as this of sediment waves at the toe of the South China Sea continental slope, southwest Taiwan (Gong et al., 2012). In contrast with the latter geometries, the crests of Type C undulations are characterised by their curved shape in plan view, and are generally parallel or sub-parallel to the bathymetric contours (Figs. 2 and 3). We thus consider unlikely that bottom currents are responsible for the Type C undulations.

In recent years, an increasingly larger number of studies have considered internal waves as a formation mechanism for the generation of seafloor sediment waves (Karl et al., 1986; Reeder et al., 2011; Ribó et al., 2016). In fact, the South China Sea hosts the largest internal waves observed in the world's oceans (Li et al., 2011; Alford et al.,

2015) (Fig. 1). They are the result of the interaction between strong tidal currents and the abrupt local bathymetry (Zhao et al., 2004; Li et al., 2008). Several fields of sediment wave have been reported on the continental shelf and slope off the Dongsha Islands, and they were interpreted as generated by internal waves interacting with the continental margin (Reeder et al., 2011; Ma et al., 2016).Our study area is just located on the western continental slope of the Dongsha Islands (Fig. 1), where internal waves have been documented by Ma et al.(2016). This indicates that the seafloor undulations in the canyon head areas might be produced by internal waves.

The breaking of internal waves on slope surfaces can create intense turbulence near the seafloor, generating local bottom currents with sufficient strength to resuspend and transport sediment (Bogucki and Redekopp, 1999; Ribbe and Holloway, 2001; Reeder et al., 2011). Moreover, internal waves' energy may be amplified at the canyon heads, as documented in the Hudson Canyon on the US Atlantic margin (Hotchkiss and Wunsch, 1982), and the Navarinsky Canyon in the Bering Sea (Karl et al., 1986). Consequently, when internal waves interact with the heads of the submarine canyons, they can become unstable, break and transfer wave energy to generate intense turbulence near the seafloor (Reeder et al., 2011; Pomar et al., 2012; Ribóet al., 2016). These seafloor-fluid mixtures, under the action of gravity, move downslope (Hotchkiss and Wunsch, 1982; Karl et al., 1986; Pomar et al., 2012).

A recent study by Ma et al. (2016) indicates that two types of sand waves can be discerned near the shelf break of the northern South China Sea. The crests of sand waves generated by internal tides are parallel to the isobaths, and are similar to the

421 crests in the canyon heads of our study area (Fig. 3b). A primary question about the
422 observed internal waves is how were they generated. Two sources of internal waves
423 have been observed in the northern South China Sea. Based on remote sensing images,
424 internal waves have been related to tidal action and Kuroshio current flow over the
425 Luzon Strait on the eastern margin of the South China Sea (Zhao et al., 2004; Li et al.,
426 2008). The other source of internal waves in the South China Sea is associated to the
427 shelf break, which records incident trans-basin waves and internal tides (Guo et al.,
428 2012; Reeder et al., 2011).

429 We infer that the Type C undulations identified in this work are most likely
430 generated by internal waves. The source of these internal waves cannot be confirmed
431 due to the lack of field measurements. In addition, when internal tides propagate, their
432 energy dissipates because of inherent mixing processes in the ocean, accompanied by
433 the generation of internal solitary waves (Guo et al., 2012). Therefore, more work is
434 needed (e.g.*in situ* measurements and numerical simulations) to determine the source
435 of the internal waves affecting the canyon head areas.

436

437 **5.2. Significance of widespread seafloor undulations to geohazard assessments in**
438 **the Pearl River Mouth Basin**

439

440 The formation of seafloor undulations has been attributed to a variety of
441 sedimentary, tectonic, and gravitational processes (Cartigny et al., 2011; Shillington et
442 al., 2012). It is of great significance to correctly pinpoint the origin of seafloor

443 undulations as they are essential for understanding the oceanographic, sedimentary,
444 and tectonic evolution of basins and margins and, particularly, for assessing
445 geohazards related to slope instability (Shillington et al., 2012). The Pearl River
446 Mouth Basin is one of the most important hydrocarbon-rich basins in the northern
447 South China Sea and has been the focus of hydrocarbon expeditions and academic
448 drilling (ODP Site 1148, IODP Expedition 349) for the past two decades (Li et al.,
449 2005; Li et al., 2014). The submarine canyon area is also a target area for gas-hydrate
450 exploration, e.g. the Shenhu area between Canyons C9 and C11 (Guan and Liang,
451 2018).

452 In this study, three different types of seafloor undulations (Types A, B and C)
453 (Fig. 12) have been identified in the submarine canyons**.** These seafloor undulations
454 show very similar morphologies on the bathymetric maps in Figs. 2 and 3. However,
455 the internal architectures of these undulations are markedly different. Internal seismic
456 reflections within Types A and C undulations are continuous and all show an apparent
457 upslope migrating pattern (Figs. 7,10 and 11). Types A and C sediment waves are
458 purely generated by sedimentary processes (turbidity currents and internal waves).
459 They are interpreted as the result of turbidity currents flowing within submarine
460 canyons and internal waves interacting with the continental slope, respectively.
461 However, their downslope flanks are quite steep (reaching 8 degrees) and show
462 lengths of up to 700m. As such, the downslope flanks can be preferential areas for
463 slope instability. Type B undulations are the seafloor manifestations of gravity-driven
464 submarine creeping, and resemble the creep folds documented by Shillington et al.

(2012) and Li et al. (2016a). They are commonly associated with listric faults, which act as potential glide planes for future slope instability (e.g. Li et al., 2016a). Resulting submarine landslides can pose catastrophic risks to oil and gas exploration and development (e.g. Piper et al., 1999). Therefore, more studies are required to determine the exact distribution of Type B seafloor undulations in the multiple submarine canyon systems of the northern South China Sea.

6 Conclusions

High-resolution 2D and 3D seismic data allowed us to investigate the morphology, internal architecture and origin of widespread seafloor undulations in the eastern area of a submarine canyon system, northern South China Sea. The main conclusions of this work are as follows:

(1) Seafloor undulations are distributed through canyon flanks, thalwegs and canyon-head areas. These seafloor undulations on the canyon flanks and thalwegs have wavelengths up to 2 km and heights up to 100 m. The wavelengths and wave heights on the canyon head areas are up to 1.5 km and 50m, respectively.

(2) All identified undulations have similar morphologies on bathymetric maps, but the three different types of seafloor undulations (Types A, B and C) can be determined based on their relative locations and internal characters. Type A undulations occur mainly in the canyon thalwegs, and their internal seismic reflections are continuous, showing an apparent upslope migrating trend. Seismic

reflections within Type B undulations are not continuous, but separated by listric faults. Type C undulations are observed in the canyon heads and their crests are roughly parallel to the local bathymetry.

(3) Types A and C undulations are sediment waves purely generated by sedimentary processes. Type A sediment waves are formed by turbidity currents flowing through the submarine canyons. Type C sediment waves most likely result from internal waves, which are amplified in the canyon heads, interacting with the continental slope. Type B undulations result from the gravity-driven (downslope) submarine creeping.

(4) To correctly identify the origin, formation processes and distribution of sediment waves in the submarine canyon systems off South China will be of great significance for future geohazard assessments in what is a hydrocarbon-rich basin of the South China Sea.

Acknowledgements

We thank China National Offshore Oil Corporation for their permission to release the seismic data. This work was financially supported by the National Scientific Foundation of China (Grant No. 41876054) and the Key Laboratory of Ocean and Marginal Sea Geology, Chinese Academy of Sciences (Grant No. OMG18-09). We thank Prof. Puig Pere and Prof. Mike Blum for valuable discussion. Dr. Wei Li is funded by the CAS Pioneer Hundred Talents Program. This paper benefited from the constructive comments of the editor (Prof. Shu Gao), Dr. Chenglin Gong and two

anonymous reviewers.

References

Alford, M.H., Peacock, T., MacKinnon, J.A., Nash, J.D., Buijsman, M.C., Centuroni, L.R., Chao, S.-Y., Chang, M.-H., Farmer, D.M., Fringer, O.B., Fu, K.-H., Gallacher, P.C., Graber, H.C., Helfrich, K.R., Jachec, S.M., Jackson, C.R., Klymak, J.M., Ko, D.S., Jan, S., Johnston, T.M.S., Legg, S., Lee, I.H., Lien, R.-C., Mercier, M.J., Moum, J.N., Musgrave, R., Park, J.-H., Pickering, A.I., Pinkel, R., Rainville, L., Ramp, S.R., Rudnick, D.L., Sarkar, S., Scotti, A., Simmons, H.L., St Laurent, L.C., Venayagamoorthy, S.K., Wang, Y.-H., Wang, J., Yang, Y.J., Paluszkiewicz, T., Tang, T.-Y., 2015. The formation and fate of internal waves in the South China Sea. Nature 521, 65-U381.

Alves, T.M., Gawthorpe, R.L., Hunt, D.W., Monteiro, J.H., 2003. Cenozoic tectono-sedimentary evolution of the western Iberian margin. Marine Geology 195, 75-108.

Baldwin, K.E., Mountain, G.S., Rosenthal, Y., 2017. Sediment waves in the Caroline Basin suggest evidence for Miocene shifts in bottom water flow in the western equatorial Pacific. Marine Geology 393, 194-202.

Belde, J., Reuning, L., Back, S., 2017. Bottom currents and sediment waves on a shallow carbonate shelf, Northern Carnarvon Basin, Australia. Continental Shelf Research 138, 142-153.

Bogucki, D.J., Redekopp, L.G., 1999. A mechanism for sediment resuspension by

internal solitary waves. Geophysical Research Letters 26, 1317-1320.

Canals, M., Puig, P., de Madron, X.D., Heussner, S., Palanques, A., Fabres, J., 2006. Flushing submarine canyons. Nature 444, 354-357.

Cartigny, M.J.B., Postma, G., van den Berg, J.H., Mastbergen, D.R., 2011. A comparative study of sediment waves and cyclic steps based on geometries, internal structures and numerical modeling. Marine Geology 280, 40-56.

Ceramicola, S., Rebesco, M., De Batist, M., Khlystov, O., 2001. Seismic evidence of small-scale lacustrine drifts in Lake Baikal (Russia). Marine Geophysical Researches 22, 445-464.

Chen, C.T.A., 2005. Tracing tropical and intermediate waters from the South China Sea to the Okinawa Trough and beyond. Journal of Geophysical Research-Oceans 110, C05012.

Chen, C.T.A., Wang, S.L., 1998. Influence of intermediate water in the western Okinawa Tough by the outflow from the South China Sea. Journal of Geophysical Research-Oceans 103, 12683-12688.

Chen, D.X., Wang, X.J., Völker, D., Wu, S.G., Wang, L., Li, W., Li, Q.P., Zhu, Z.Y., Li, C.L., Qin, Z.L., Sun, Q.L., 2016. Three dimensional seismic studies of deep-water hazard-related features on the northern slope of South China Sea. Marine and Petroleum Geology 77, 1125-1139.

Chen, H., Xie, X.N., Van Rooij, D., Vandorpe, T., Su, M., Wang, D.X., 2014. Depositional characteristics and processes of alongslope currents related to a seamount on the northwestern margin of the Northwest Sub-Basin, South China

553 Sea. Marine Geology 355, 36-53.
554 Chen, H.J., Zhan, W.H., Li, L.Q., Wen, M.M., 2017. Occurrence of submarine
555 canyons, sediment waves and mass movements along the northern continental
556 slope of the South China Sea. Journal of Earth System Science 126, 73.
557 Damuth, J.E., 1979. Migrating sediment waves created by turbidity currents in the
558 northern South China Basin. Geology 7, 520-523.
559 Dong, D.D., Zhang, G.C., Zhong, K., Yuan, S.Q., Wu, S.G., 2009. Tectonic Evolution
560 and Dynamics of Deepwater Area of Pearl River Mouth Basin, Northern South
561 China Sea. Journal of Earth Science 20, 147-159.
562 Droghei, R., Falcini, F., Casalbore, D., Martorelli, E., Mosetti, R., Sannino, G.,
563 Santoleri, R., Chiocci, F.L., 2016. The role of Internal Solitary Waves on
564 deep-water sedimentary processes: the case of up-slope migrating sediment
565 waves off the Messina Strait. Scientific Reports 6.
566 https://doi.org/10.1038/srep36376.
567 Ercilla, G., Wynn, R.B., Alonso, B., Baraza, J., 2002. Initiation and evolution of
568 turbidity current sediment waves in the Magdalena turbidite system. Marine
569 Geology 192, 153-169.
570 Faugères, J.C., Gonthier, E., Mulder, T., Kenyon, N., Cirac, P., Griboulard, R., Berne,
571 S., Lesuave, R., 2002. Multi-process generated sediment waves on the Landes
572 Plateau (Bay of Biscay, North Atlantic). Marine Geology 182, 279-302.
573 Flood, R.D., Shor, A.N., Manley, P.L., 1993. Morphology of abyssal mudwaves at
574 Project MUDWAVES sites in the Argentine Basin. Deep-Sea Research Part

Ii-Topical Studies in Oceanography 40, 859-888.

Gong, C.L., Wang, Y.M., Peng, X.C., Li, W.G., Qiu, Y., Xu, S., 2012. Sediment waves on the South China Sea Slope off southwestern Taiwan: Implications for the intrusion of the Northern Pacific Deep Water into the South China Sea. Marine and Petroleum Geology 32, 95-109.

Gong, C.L., Wang, Y.M., Rebesco, M., Salon, S., Steel, R.J., 2018. How do turbidity flows interact with contour currents in unidirectionally migrating deep-water channels? Geology 46, 551-554.

Gong, C.L., Wang, Y.M., Zhu, W.L., Li, W.G., Xu, Q., 2013. Upper Miocene to Quaternary unidirectionally migrating deep-water channels in the Pearl River Mouth Basin, northern South China Sea. Aapg Bulletin 97, 285-308.

Gonthier, E., Faugères, J.C., Gervais, A., Ercilla, G., Alonso, B., Baraza, J., 2002. Quaternary sedimentation and origin of the Orinoco sediment–wave field on the Demerara continental rise (NE margin of South America). Marine Geology 192, 189-214.

Guan, J.A., Liang, D.Q., 2018. Discussion on the rapid formation mechanism and evolution process of methane hydrate-bearing sediments in Shenhu Area of northern South China Sea. Marine and Petroleum Geology 91, 225-235.

Guo, P., Fang, W.D., Liu, C.J., Qiu, F.W., 2012. Seasonal characteristics of internal tides on the continental shelf in the northern South China Sea. Journal of Geophysical Research-Oceans 117, C04023.

He, Y., Zhong, G.F., Wang, L.L., Kuang, Z.G., 2014. Characteristics and occurrence

of submarine canyon-associated landslides in the middle of the northern continental slope, South China Sea. Marine and Petroleum Geology 57, 546-560.

Hill, P.R., Moran, K.M., Blasco, S.M., 1982. Creep deformation of slope sediments in the Canadian Beaufort Sea. Geo-Marine Letters 2, 163-170.

Hotchkiss, F.S., Wunsch, C., 1982. Internal waves in Hudson Canyon with possible geological implications. Deep Sea Research Part A. Oceanographic Research Papers 29, 415-442.

Jiang, J., Shi, H.S., Lin, C.S., Zhang, Z.T., Wei, A., Zhang, B., Shu, L.F., Tian, H.X., Tao, Z., Liu, H.Y., 2017. Sequence architecture and depositional evolution of the Late Miocene to quaternary northeastern shelf margin of the South China Sea. Marine and Petroleum Geology 81, 79-97.

Jiang, T., Xie, X.N., Wang, Z.F., Li, X.S., Zhang, Y.Z., Sun, H., 2013. Seismic features and origin of sediment waves in the Qiongdongnan Basin, northern South China Sea. Marine Geophysical Research 34, 281-294.

Karl, H.A., Cacchione, D.A., Carlson, P.R., 1986. Internal-wave currents as a mechanism to account for large sand waves in Navarinsky Canyon head, Bering Sea. Journal of Sedimentary Petrology 56, 706-714.

Kuang, Z.G., Zhong, G.F., Wang, L.L., Guo, Y.Q., 2014. Channel-related sediment waves on the eastern slope offshore Dongsha Islands, northern South China Sea. Journal of Asian Earth Sciences 79, 540-551.

Lee, S.H., Chough, S.K., 2001. High-resolution (2-7 kHz) acoustic and geometric characters of submarine creep deposits in the South Korea Plateau, East Sea.

619 Sedimentology 48, 629-644.
620 Lewis, K.B., Pantin, H.M., 2002. Channel-axis, overbank and drift sediment waves in
621 the southern Hikurangi Trough, New Zealand. Marine Geology 192, 123-151.
622 Li, C.F., Xu, X., Lin, J., Sun, Z., Zhu, J., Yao, Y.J., Zhao, X.X., Liu, Q.S., Kulhanek,
623 D.K., Wang, J., Song, T.R., Zhao, J.F., Qiu, N., Guan, Y.X., Zhou, Z.Y., Williams,
624 T., Bao, R., Briais, A., Brown, E.A., Chen, Y.F., Clift, P.D., Colwell, F.S., Dadd,
625 K.A., Ding, W.W., Almeida, I.H., Huang, X.L., Hyun, S., Jiang, T., Koppers,
626 A.A.P., Li, Q.Y., Liu, C.L., Liu, Z.F., Nagai, R.H., Peleo-Alampay, A., Su, X.,
627 Tejada, M.L.G., Trinh, H.S., Yeh, Y.C., Zhang, C.L., Zhang, F., Zhang, G.L.,
628 2014. Ages and magnetic structures of the South China Sea constrained by deep
629 tow magnetic surveys and IODP Expedition 349. Geochemistry, Geophysics,
630 Geosystems 15, 4958-4983.
631 Li, D., Chen, X., Liu, A., 2011. On the generation and evolution of internal solitary
632 waves in the northwestern South China Sea. Ocean Modelling 40, 105-119.
633 Li, Q.Y., Jian, Z.M., Su, X., 2005. Late Oligocene rapid transformations in the South
634 China Sea. Marine Micropaleontology 54, 5-25.
635 Li, W., Alves, T.M., Wu, S.G., Rebesco, M., Zhao, F., Mi, L.J., Ma, B.J., 2016a. A
636 giant, submarine creep zone as a precursor of large-scale slope instability
637 offshore the Dongsha Islands (South China Sea). Earth and Planetary Science
638 Letters 451, 272-284.
639 Li, X.F., Zhao, Z.X., Pichel, W.G., 2008. Internal solitary waves in the northwestern
640 South China Sea inferred from satellite images. Geophysical Research Letters 35.

641 https://doi.org/10.1029/2008GL034272.
642 Li, X.S., Liu, L.J., Li, J.G., Gao, S., Zhou, Q.J., Su, T.Y., 2015. Mass movements in
643 small canyons in the northeast of Baiyun deepwater area, north of the South
644 China Sea. Acta Oceanologica Sinica 34, 35-42.
645 Li, X.S., Zhou, Q.J., Su, T.Y., Liu, L.J., Gao, S., Zhou, S.W., 2016b. Slope-confined
646 submarine canyons in the Baiyun deep-water area, northern South China Sea:
647 variation in their modern morphology. Marine Geophysical Research 37, 95-112.
648 Ludmann, T., Wong, H.K., Berglar, K., 2005. Upward flow of North Pacific Deep
649 Water in the northern South China Sea as deduced from the occurrence of drift
650 sediments. Geophysical Research Letters 32, L05614.
651 Ma, B.J., Wu, S.G., Sun, Q.L., Mi, L.J., Wang, Z.Z., Tian, J., 2015. The late Cenozoic
652 deep-water channel system in the Baiyun Sag, Pearl River Mouth Basin:
653 Development and tectonic effects. Deep Sea Research Part II: Topical Studies in
654 Oceanography 122, 226-239.
655 Ma, X.C., Yan, J., Hou, Y.J., Lin, F.L., Zheng, X.F., 2016. Footprints of obliquely
656 incident internal solitary waves and internal tides near the shelf break in the
657 northern South China Sea. Journal of Geophysical Research-Oceans 121,
658 8706-8719.
659 Masson, D.G., Howe, J.A., Stoker, M.S., 2002. Bottom-current sediment waves,
660 sediment drifts and contourites in the northern Rockall Trough. Marine Geology
661 192, 215-237.
662 McCave, I.N., 2017. Formation of sediment waves by turbidity currents and

663 geostrophic flows: A discussion. Marine Geology 390, 89-93.
664 Normark, W.R., Hess, G.R., Stow, D.A.V., Bowen, A.J., 1980. Sediment waves on the
665 monterey fan levee: A preliminary physical interpretation. Marine Geology 37,
666 1-18.
667 Normark, W.R., Piper, D.J.W., Posamentier, H., Pirmez, C., Migeon, S., 2002.
668 Variability in form and growth of sediment waves on turbidite channel levees.
669 Marine Geology 192, 23-58.
670 Parker, G., 1982. Conditions for the ignition of catastrophically erosive turbidity
671 currents. Marine Geology 46, 307-327.
672 Paull, C.K., Talling, P.J., Maier, K.L., Parsons, D., Xu, J.P., Caress, D.W., Gwiazda,
673 R., Lundsten, E.M., Anderson, K., Barry, J.P., Chaffey, M., O'Reilly, T.,
674 Rosenberger, K.J., Gales, J.A., Kieft, B., McGann, M., Simmons, S.M., McCann,
675 M., Sumner, E.J., Clare, M.A., Cartigny, M.J., 2018. Powerful turbidity currents
676 driven by dense basal layers. Nature Communications 9, Article number: 4114.
677 Perez-Hernandez, S., Comas, M.C., Escutia, C., 2014. Morphology of turbidite
678 systems within an active continental margin (the Palomares Margin, western
679 Mediterranean). Geomorphology 219, 10-26.
680 Piper, D.J.W., Cochonat, P., Morrison, M., 1999. The sequence of events around the
681 epicentre of the 1929 grand banks earthquake: initiation of debris flows and
682 turbidity currents inferred from sidescan sonar. Sedimentology 46, 79–97.
683 Pomar, L., Morsilli, M., Hallock, P., Bádenas, B., 2012. Internal waves, an
684 under-explored source of turbulence events in the sedimentary record.

685 Earth-Science Reviews 111, 56-81.
686 Pope, E.L., Jutzeler, M., Cartigny, M.J.B., Shreeve, J., Tailing, P.J., Wright, I.C.,
687 Wysoczanski, R.J., 2018. Origin of spectacular fields of submarine sediment
688 waves around volcanic islands. Earth and Planetary Science Letters 493, 12-24.
689 Qiao, S.H., Su, M., Kuang, Z.G., Yang, R., Liang, J.Q., Wu, N.Y., 2015.
690 Canyon-related undulation structures in the Shenhu area, northern South China
691 Sea. Marine Geophysical Research 36, 243-252.
692 Rebesco, M., Camerlenghi, A., Volpi, V., Neagu, C., Accettella, D., Lindberg, B.,
693 Cova, A., Zgur, F., 2007. Interaction of processes and importance of contourites:
694 insights from the detailed morphology of sediment Drift 7, Antarctica.
695 Geological Society, London, Special Publications 276, 95-110.
696 Rebesco, M., Neagu, R.C., Cuppari, A., Muto, F., Accettella, D., Dominici, R., Cova,
697 A., Romano, C., Caburlotto, A. 2009. Morphobathymetric analysis and evidence
698 of submarine mass movements in the western Gulf of Taranto (Calabria margin,
699 Ionian Sea). International Journal of Earth Sciences 98, 791-805.
700 Reeder, D.B., Ma, B.B., Yang, Y.J., 2011. Very large subaqueous sand dunes on the
701 upper continental slope in the South China Sea generated by episodic, shoaling
702 deep-water internal solitary waves. Marine Geology 279, 12-18.
703 Ribó, M., Durán, R., Puig, P., Van Rooij, D., Guillén, J., Masqué, P., 2018. Large
704 sediment waves over the Gulf of Roses upper continental slope (NW
705 Mediterranean). Marine Geology 399, 84-96.
706 Ribó, M., Puig, P., Muñoz, A., Lo Iacono, C., Masqué, P., Palanques, A., Acosta, J.,

Guillén, J., Gómez Ballesteros, M., 2016. Morphobathymetric analysis of the large fine-grained sediment waves over the Gulf of Valencia continental slope (NW Mediterranean). Geomorphology 253, 22-37.

Ribbe, J., Holloway, P.E., 2001. A model of suspended sediment transport by internal tides. Continental Shelf Research 21, 395-422.

Shepard, F.P., 1981. Submarine Canyons: Multiple Causes and Long-Time Persistence. Aapg Bulletin-American Association of Petroleum Geologists 65, 1062-1077.

Shillington, D.J., Seeber, L., Sorlien, C.C., Steckler, M.S., Kurt, H., Dondurur, D., Cifci, G., Imren, C., Cormier, M.H., McHugh, C.M.G., Gurcay, S., Poyraz, D., Okay, S., Atgin, O., Diebold, J.B., 2012. Evidence for widespread creep on the flanks of the Sea of Marmara transform basin from marine geophysical data. Geology 40, 439-442.

Sultan, N., Cochonat, P., Canals, M., Cattaneo, A., Dennielou, B., Haflidason, H., Laberg, J.S., Long, D., Mienert, J., Trincardi, F., Urgeles, R., Vorren, T.O., Wilson, C., 2004. Triggering mechanisms of slope instability processes and sediment failures on continental margins: a geotechnical approach. Marine Geology 213, 291-321.

Sun, Q.L., Alves, T., Xie, X.N., He, J.X., Li, W., Ni, X.L., 2017. Free gas accumulations in basal shear zones of mass-transport deposits (Pearl River Mouth Basin, South China Sea): An important geohazard on continental slope basins. Marine and Petroleum Geology 81, 17-32.

Sun, Q.L., Wu, S.G., Cartwright, J., Dong, D.D., 2012. Shallow gas and focused fluid

729 flow systems in the Pearl River Mouth Basin, northern South China Sea. Marine
730 Geology 315-318, 1-14.
731 Symons, W.O., Sumner, E.J., Tailing, P.J., Cartigny, M.J.S., Clare, M.A., 2016.
732 Large-scale sediment waves and scours on the modern seafloor and their
733 implications for the prevalence of supercritical flows. Marine Geology 371,
734 130-148.
735 Talling, P.J., Allin, J., Armitage, D.A., Arnott, R.W.C., Cartigny, M.J.B., Clare, M.A.,
736 Felletti, F., Covault, J.A., Girardclos, S., Hansen, E., Hill, P.R., Hiscott, R.N.,
737 Hogg, A.J., Clarke, J.H., Jobe, Z.R., Malgesini, G., Mozzato, A., Naruse, H.,
738 Parkinson, S., Peel, F.J., Piper, D.J.W., Pope, E., Postma, G., Rowley, P.,
739 Sguazzini, A., Stevenson, C.J., Sumner, E.J., Sylvester, Z., Watts, C., Xu, J.,
740 2015. Key future directions for research on turbidity currents and their deposits.
741 Journal of Sedimentary Research 85, 153-169.
742 Taylor, B., Hayes, D.E., 1980. The tectonic evolution of the South China Basin. In:
743 Hayes, D.E. (Ed.) The Tectonic and Geologic Evolution of Southeast Asian Seas
744 and Islands, Am. Geophys. Union Monogr. 23, 89-104.
745 Urlaub, M., Geersen, J., Krastel, S., Schwenk, T., 2018. Diatom ooze: Crucial for the
746 generation of submarine mega-slides? Geology 46, 331-334.
747 Wynn, R.B., Stow, D.A.V., 2002. Classification and characterisation of deep-water
748 sediment waves. Marine Geology 192, 7-22.
749 Wynn, R.B., Weaver, P.P.E., Ercilla, G., Stow, D.A.V., Masson, D.G., 2000.
750 Sedimentary processes in the Selvage sediment-wave field, NE Atlantic: new

751 insights into the formation of sediment waves by turbidity currents.
752 Sedimentology 47, 1181-1197.
753 Xie, X.N., Müller, R.D., Li, S., Gong, Z.S., Steinberger, B., 2006. Origin of
754 anomalous subsidence along the Northern South China Sea margin and its
755 relationship to dynamic topography. Marine and Petroleum Geology 23,
756 745-765.
757 Yang, Q.X., Tian, J.W., Zhao, W., 2010. Observation of Luzon Strait transport in
758 summer 2007. Deep Sea Research Part I: Oceanographic Research Papers 57,
759 670-676.
760 Zhao, Y.L., Liu, Z.F., Zhang, Y.W., Li, J.R., Wang, M., Wang, W.G., Xu, J.P., 2015. In
761 situ observation of contour currents in the northern South China Sea:
762 Applications for deepwater sediment transport. Earth and Planetary Science
763 Letters 430, 477-485.
764 Zhao, Z.X., Klemas, V., Zheng, Q.N., Yan, X.H., 2004. Remote sensing evidence for
765 baroclinic tide origin of internal solitary waves in the northeastern South China
766 Sea. Geophysical Research Letters 31.
767 Zhu, M.Z., Graham, S., Pang, X., McHargue, T., 2010. Characteristics of migrating
768 submarine canyons from the middle Miocene to present: Implications for
769 paleoceanographic circulation, northern South China Sea. Marine and Petroleum
770 Geology 27, 307-319.
771 Zhu, W.L., Huang, B.J., Mi, L.J., Wilkins, R.W.T., Fu, N., Xiao, X.M., 2009.
772 Geochemistry, origin, and deep-water exploration potential of natural gases in

the Pearl River Mouth and Qiongdongnan basins, South China Sea. Aapg Bulletin 93, 741-761.

Figures and Figure Captions

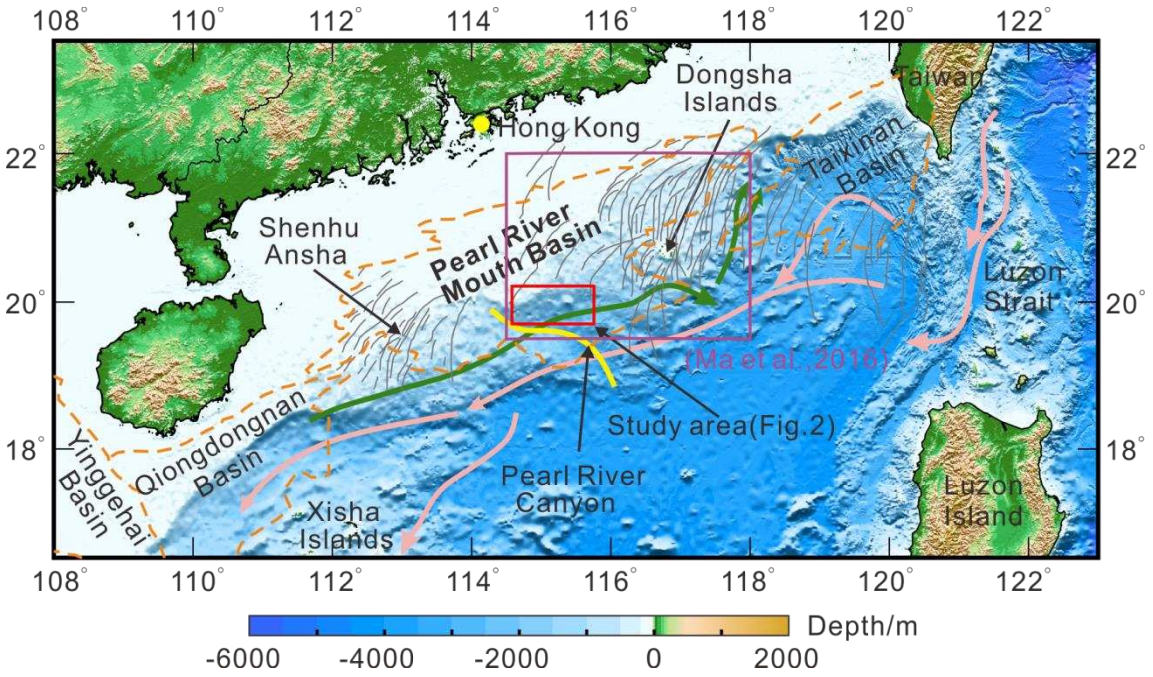

Fig.1 Bathymetric map of the northern South China Sea margin. The orange dashed lines highlight the distribution of four major deep-water sedimentary basins. The yellow curve represents the location of the Pearl River Canyon. The grey curves represent internal waves observed in satellite imagery (extracted from Zhao et al., 2004; Li et al., 2011). The red box outlines the area enlarged in Figure 2. The purple box represents extent of internal waves and the region of *in situ* current measurements (Ma et al., 2016). The green and pink arrows indicate the circulation pathways of intermediate and deep-water masses, respectively (modified after Chen et al., 2014).

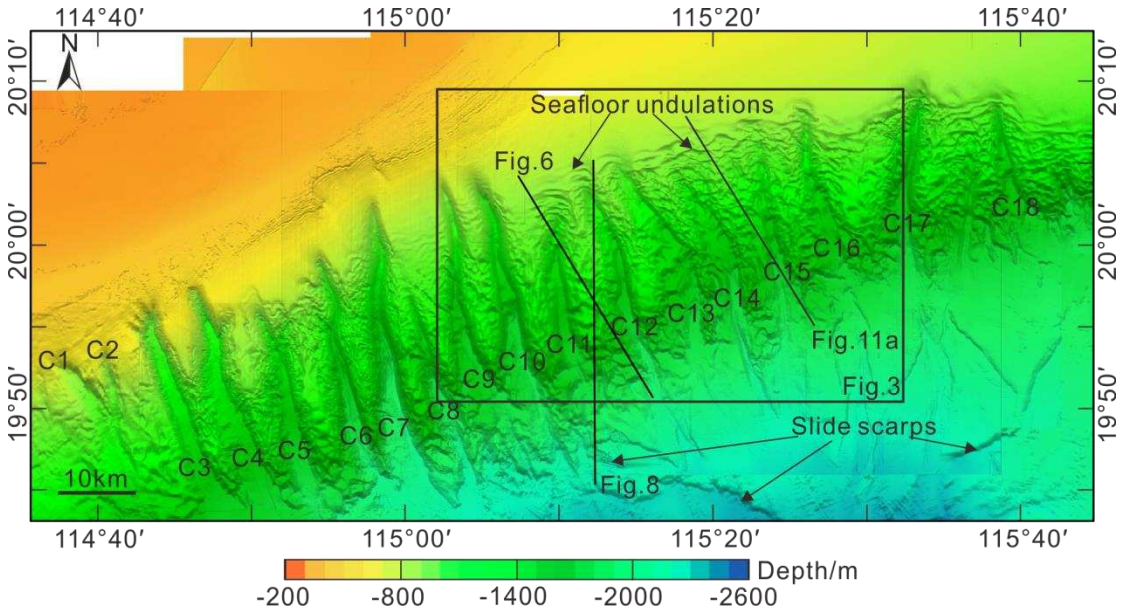

788

789 Fig. 2 High-resolution bathymetric map of the study area showing eighteen submarine
790 canyons (C1 to C18) with a NW-SE orientation. Note that the heads of C9 to C18
791 show widespread seafloor undulations. Several slide scarps are clearly identified
792 downslope from the submarine canyons. The black box represents the location of
793 Figure 3. The black lines show the location of the high-resolution seismic profiles in
794 Figures 6, 8 and 11.

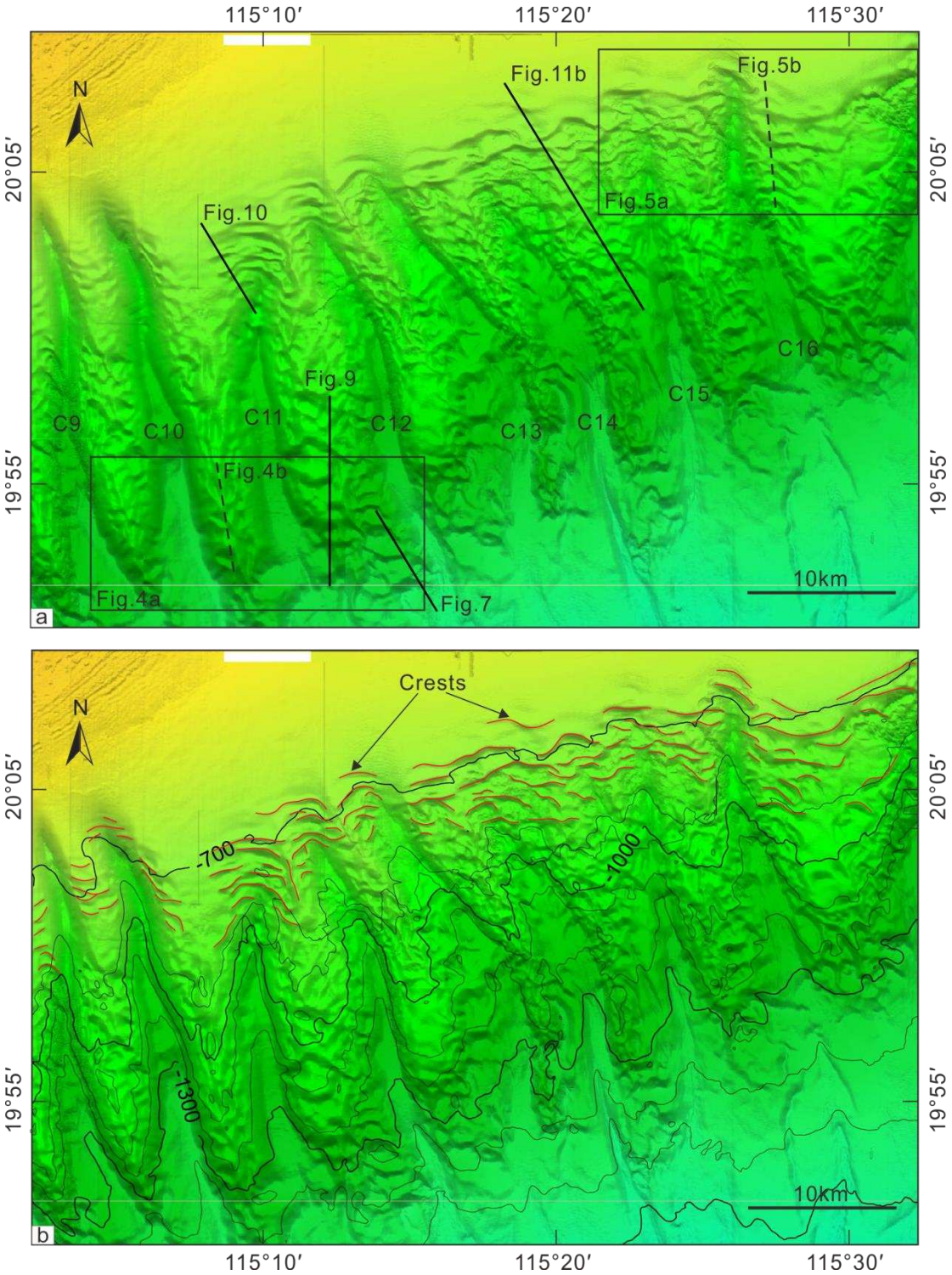

Fig. 3 (a) Bathymetric map illustrating the detailed morphology of the studied seafloor undulations. Seafloor undulations are mainly located at the heads and flanks of the submarine canyons. The black solid lines represent the locations of the 2D seismic profiles used in this study. The black dotted lines indicate the locations of

bathymetric profiles show in Figs. 4b and 5b. (b) Distribution of the crests of seafloor undulations on the bathymetric map. The crests of the seafloor undulations are show in red and are parallel or sub-parallel to the bathymetric contours. The contour interval is 100 m.

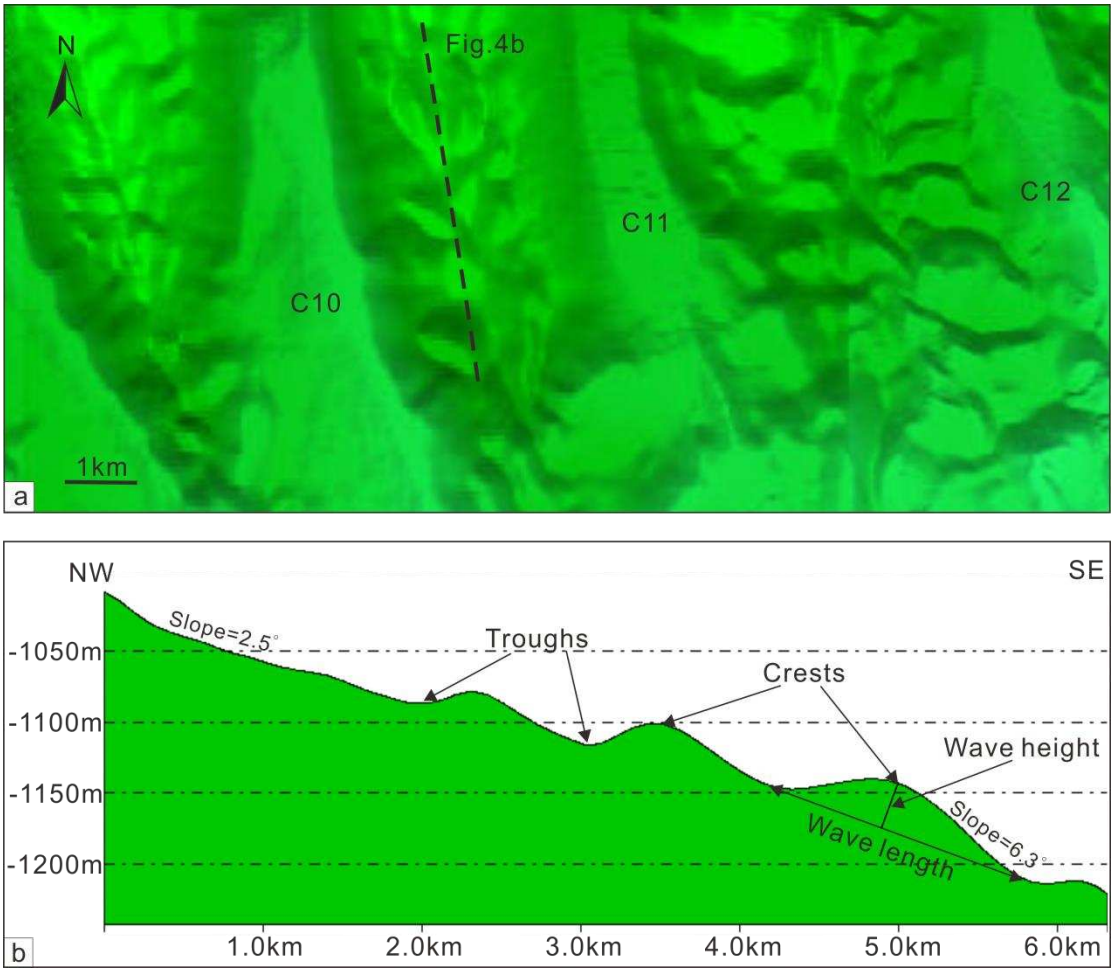

Fig. 4 (a) Bathymetric map revealing the detailed seafloor morphology of the lower flanks of submarine canyons, stressing the presence of widely distributed seafloor undulations. See Fig. 3 for the location of the bathymetric survey. (b) Bathymetric profile crossing the flank area between Canyon 10 and 11 and revealing multiple seafloor undulations. The wavelength and height of these seafloor undulations can

reach up to 2 km and 100 m, respectively.

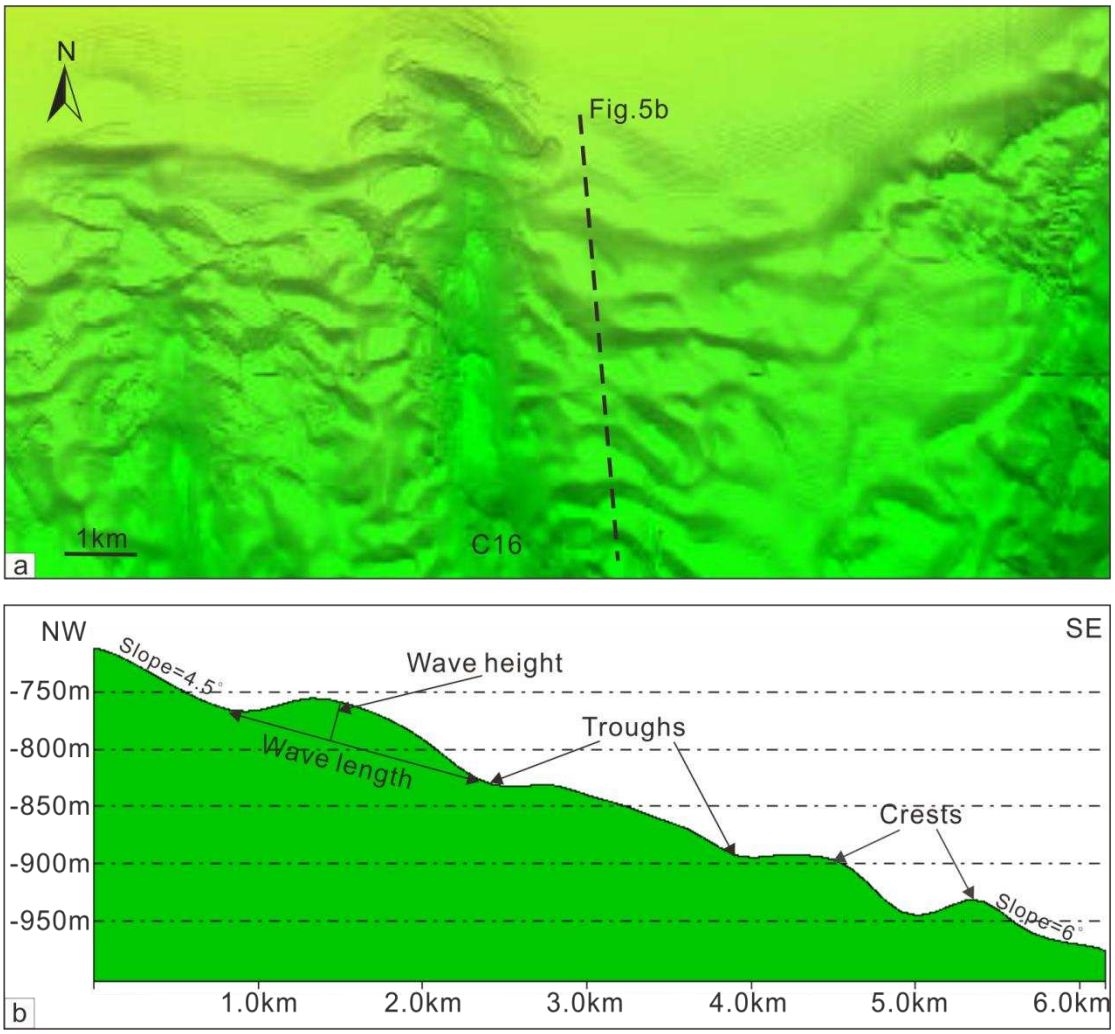

Fig. 5 (a) Bathymetric map highlighting the detailed seafloor morphology of the upper continental slope. Widespread seafloor undulations can be observed. See Fig. 3 for the location of the bathymetric survey. (b) Bathymetric profile crossing the upper ridge area between canyon 16 and 17, revealing the presence of multiple seafloor undulations. They can be up to 1.5 km in wavelength (trough to trough) and 50 m in height (maximum relief).

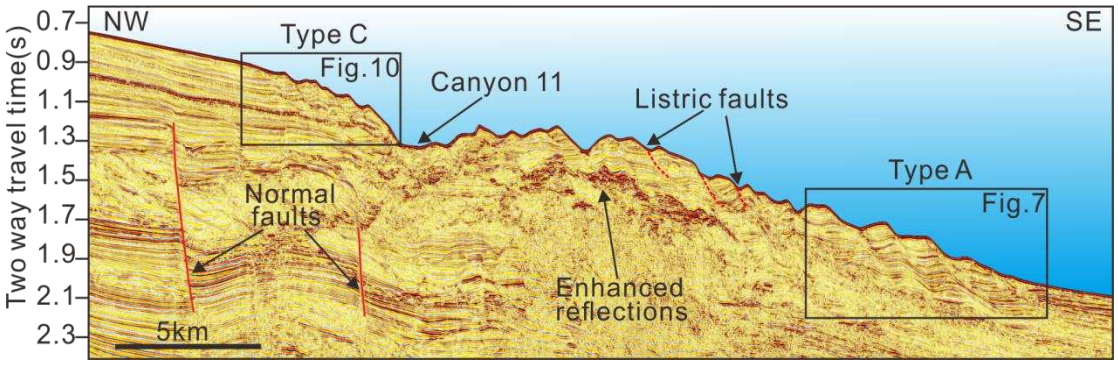

820

821 Fig. 6 Two-dimensional (2D) seismic line crossing the head of Canyon 11 and the
822 flank area between C11 and C12 (for location of the profile see Fig. 2). Several
823 large-scale normal faults and listric faults can be distinguished, which are marked by
824 red solid and dotted lines, respectively. Note the presence of high-amplitude enhanced
825 seismic reflections beneath some of the seafloor undulations.

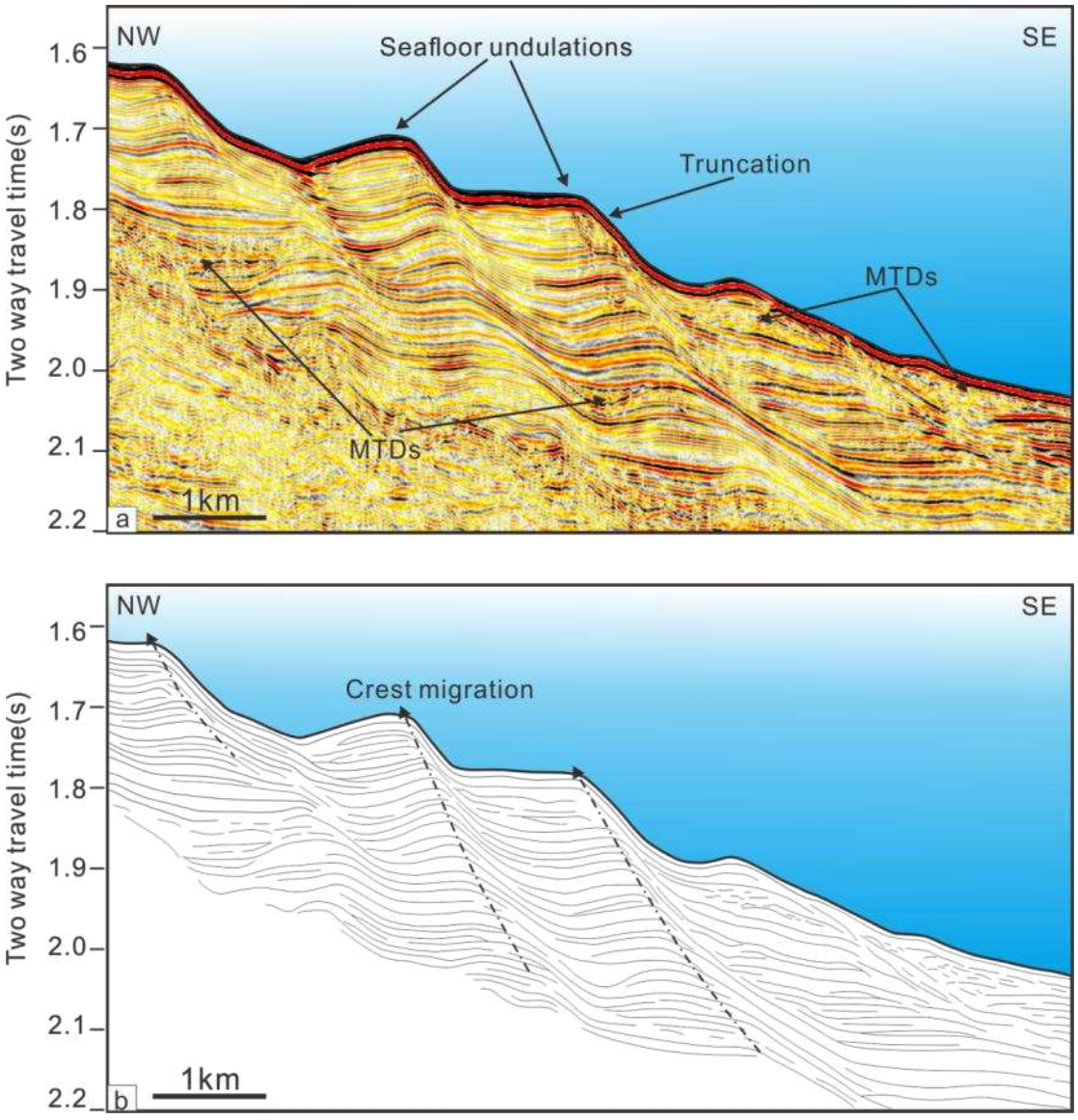

826

827 Fig. 7 (a) Zoomed section of the seismic profile in Fig. 6 revealing the detailed
828 internal character of the seafloor undulations in the lower reach of the canyon flanks,
829 between C11 and C12. Seafloor undulations are clearly observed on the seafloor and
830 their crests show an upslope migration trend. Note that the downslope flanks of most
831 of the undulated structures are steeper than their upslope counterparts. Several MTDs
832 can be distinguished within the seafloor undulations. (b) Line-drawn interpretation of
833 Fig. 7a revealing the internal seismic reflectors within the undulations, which are
834 continuous across the troughs separating distinct undulations.

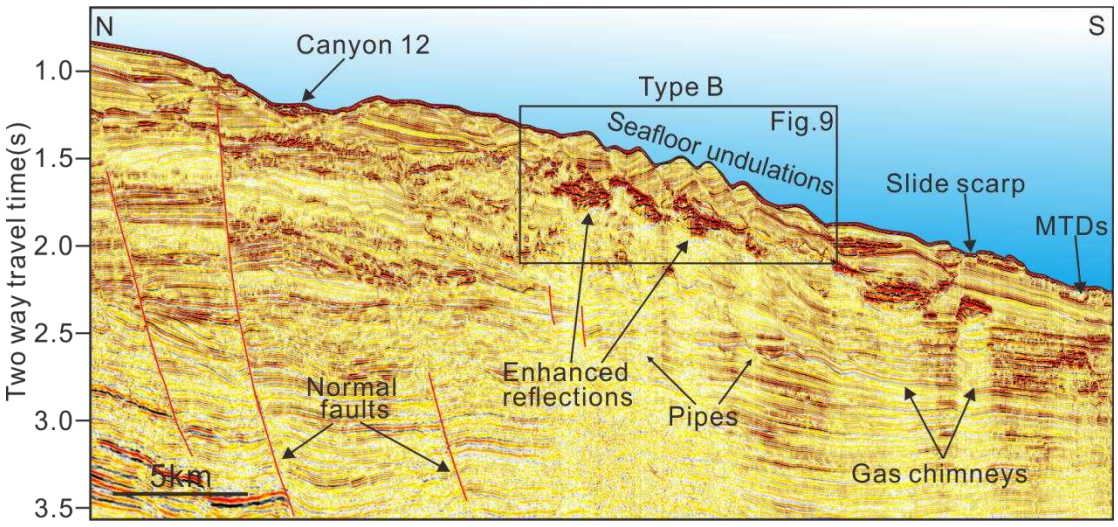

Fig. 8 High-resolution seismic profile crossing C12 and the canyon flank between C11 and C12 (for location of the profile see Fig. 2). A slide scarp and multiple seafloor undulations can be identified on the modern seafloor. Note the presence of gas chimneys, pipes and high-amplitude (enhanced) seismic reflections beneath the undulations.

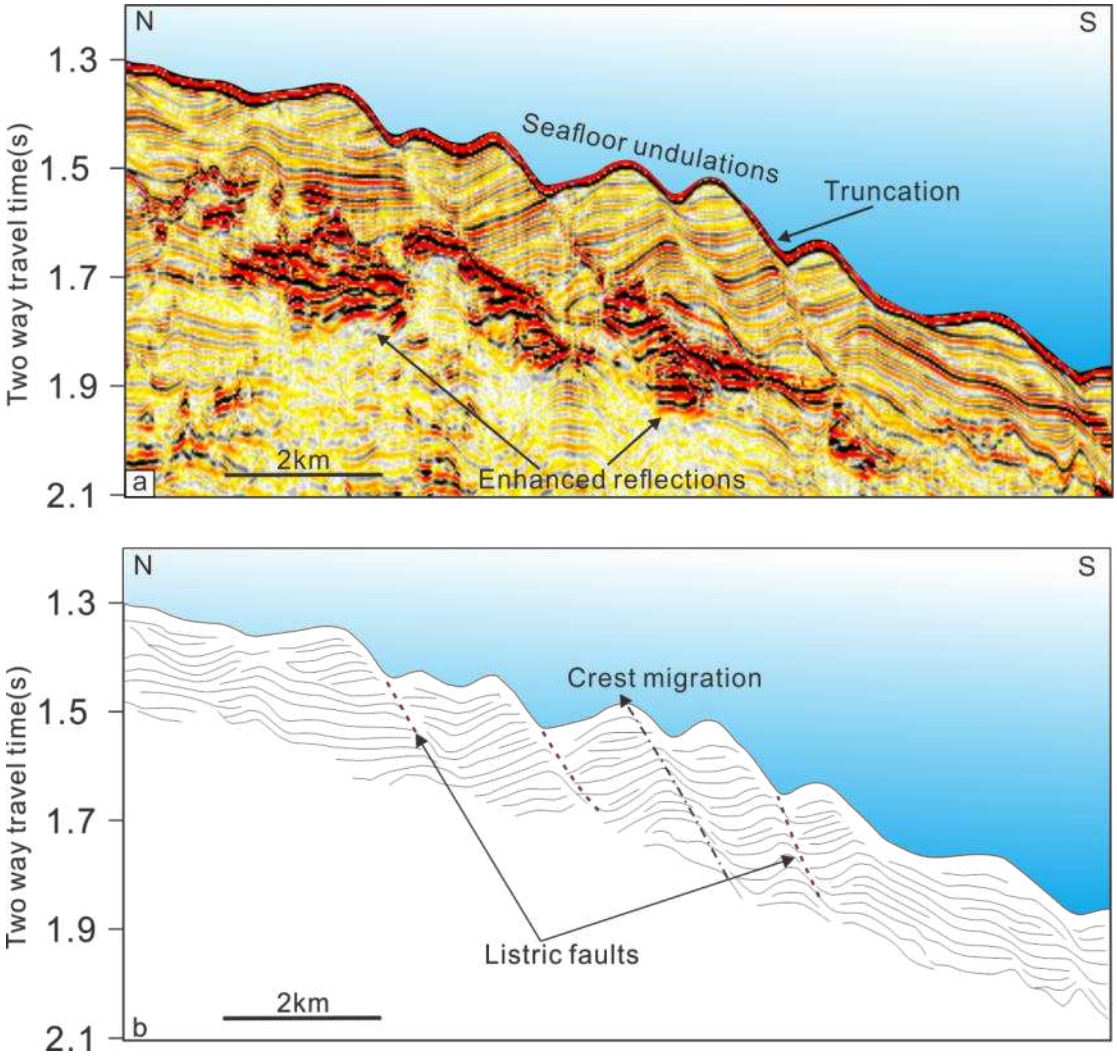

Fig. 9 (a) Zoomed section of the seismic profile in Fig. 8 showing the internal architecture of seafloor undulations on the canyon flank between C11 and C12. Seismic reflections within seafloor undulations are not continuous and cannot be traced across the troughs from one wave to the next. Most of the seafloor undulations are separated by small-scale listric faults. (b) Line-drawn interpretation of Fig. 9a illustrating the internal seismic reflections within the seafloor undulations, which are not continuous.

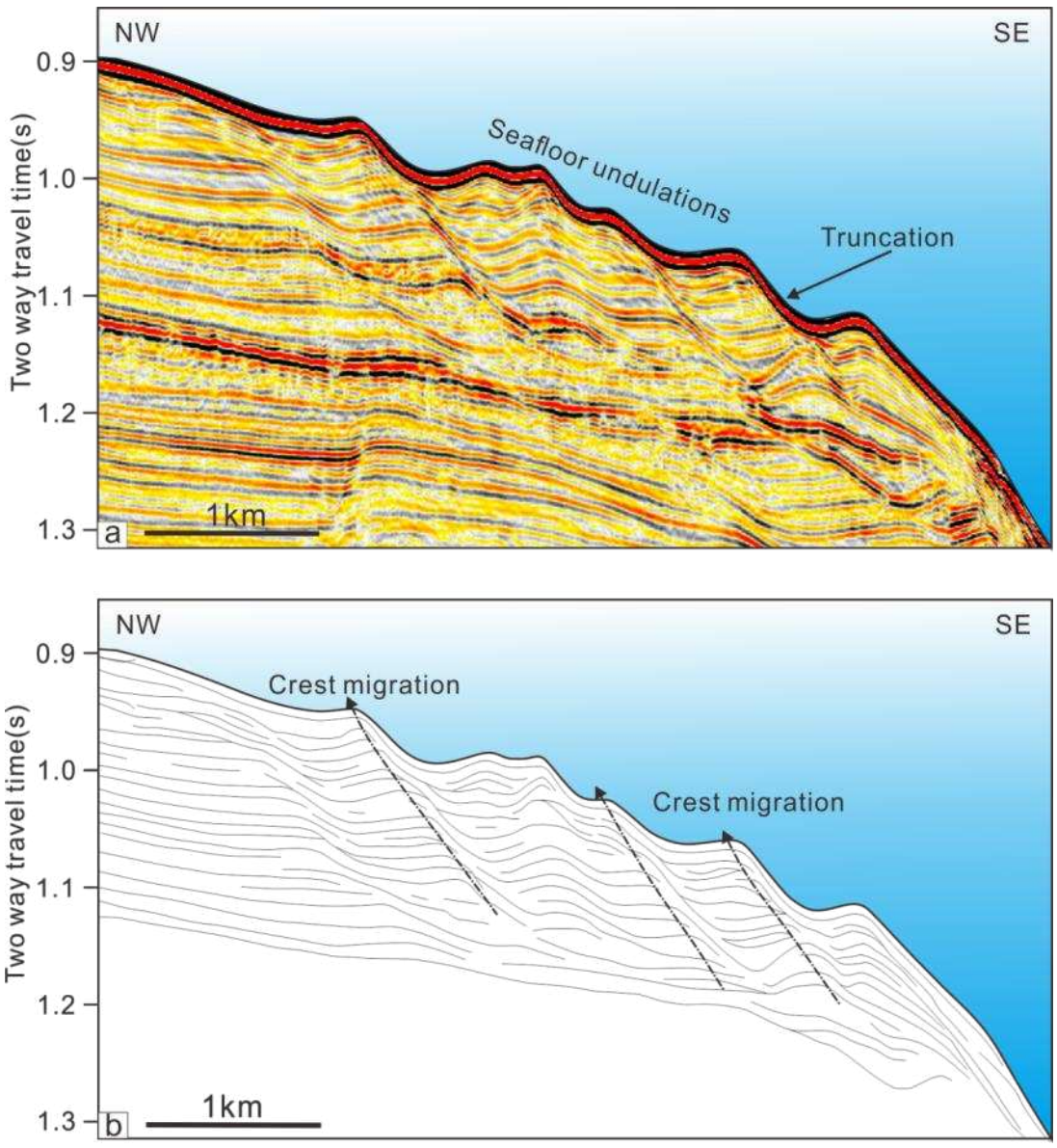

Fig.10 (a) Zoomed section of the seismic profile in Fig. 6 showing the detailed internal architecture of sediment waves at the head of C11. Internal seismic reflections within the seafloor undulations are continuous and can be traced from one wave to the next. Note that the crests of the undulated structures reveal an upslope migration pattern. (b) Line-drawn interpretation of Fig. 10a highlighting that most of the internal reflectors crossing the different seafloor undulationsare continuous.

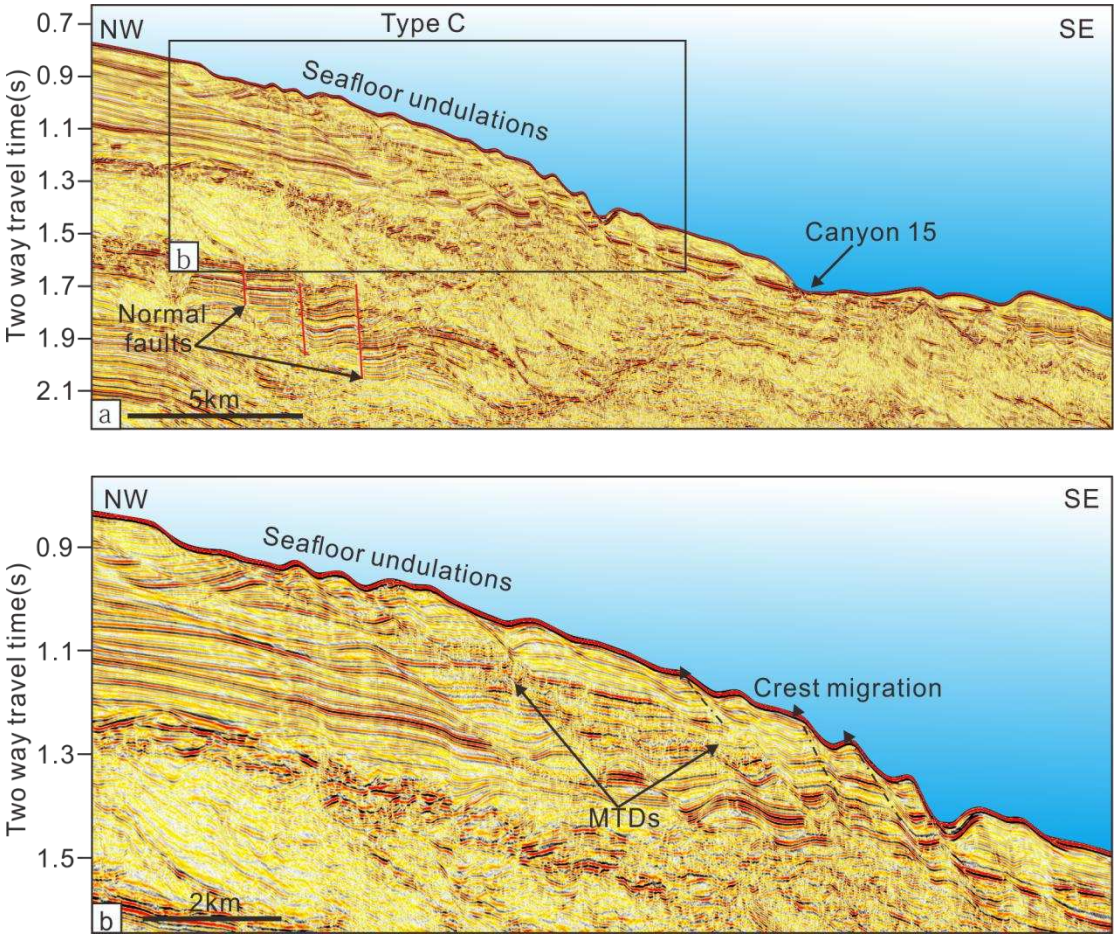

858

859 Fig. 11 (a) Two-dimensional (2D) seismic profile crossing C15 and the canyon flank
860 between C14 and C15 (see Fig. 2 for location of the profile). Multiple sediment waves
861 are observed in the canyon head. (b) Zoomed section in Fig. 11b showing the internal
862 architecture of sediment waves in the canyon head. Note that most of the sediment
863 waves show an upslope migration trend. Several MTDs can be identified within the
864 imaged sediment waves.

865

Types	Locatons	Seafloor morphology	Seismic characteristics	Line drawing	Wave-forming process
Type A	Lower of canyon thalwegs	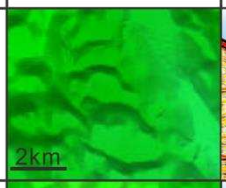	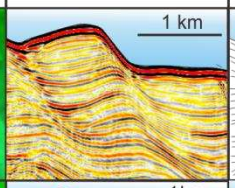	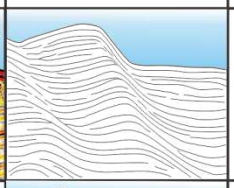	Turbidity currents
Type B	Canyon flanks	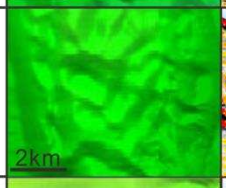	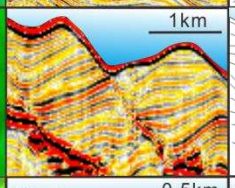	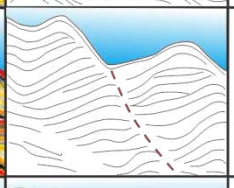	Submarine creeps
Type C	Canyon heads	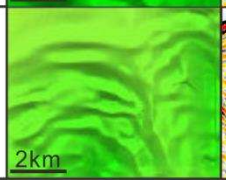	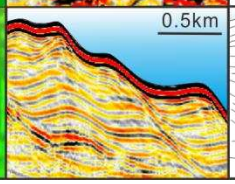	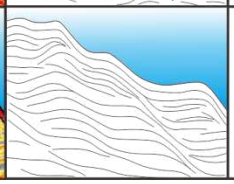	Internal waves

Fig. 12 Classification of three different types of seafloor undulations based on their location and origin. Representative seismic profiles and related line drawings illustrate the formation mechanisms of the seafloor undulations. Types A and B undulations are distributed in the canyon areas. The former are generated by turbidity currents, while the latter are generated by gravitational deformation processes (gravity-driven submarine creep). Type C undulations are mainly located at the heads of the submarine canyons and were generated by internal waves.